JAST, Vol. 6, No. 2, pp 99–113
◯ Iranian Aerospace Society, Spring 2009

JAST
Journal of Aerospace Science and Technology

Progressive Damage Analysis of Laminated Composites Using Continum Damage Mechanics

B. Mohammadi[1], H. Hosseini-Toudeshky[2], M. H. Sadr[3]

In this paper, progressive damage and global failure of composite laminates under quasi-static, monotonic loading are investigated using 3D continuum damage mechanics. For this purpose, a finite element program has been developed using an eight-node 2D layered element including layer-wise plate theory. Damage analysis of a single orthotropic layer under various uniform in-plane and transverse loading conditions, and laminate problems with diffuse damage under simply supported and distributed transverse loading conditions are performed. The effects of modeling parameters such as hardening rules and mesh densities along the laminate thickness and in-plane surface on the progressive damage response and global failure are also investigated.

INTRODUCTION

Composite structures experience local failure or damage such as matrix cracking, fiber failure, fiber–matrix shear deformation, and delamination. These forms of microscopic damage have been experimentally shown to initiate at loads that are far below the ultimate strength of the composite material. Once a microscopic damage is initiated, it tends to progress as the loading is further increased or cycled.

Most of the past efforts in modeling of the progression of distributed microscopic damage in composite laminates have relied on the use of continuum damage mechanics (CDM). Kachanov [1], Lemaitre [2-3], Chaboche [4-5] and Krajcinovic [6-7] used continuum damage mechanics to analyze different types of damage ranging from brittle fracture to ductile failure.

Talreja [8] used CDM for composite laminates by proposing two first order tensorial damage representations associated with the principal direction of material coordinate, and a specific analytical investigations of damage states without considering the growth functions or damage thresholds. In a subsequent work, he [9] applied his model to predict the stiffness reduction in a number of angle-ply laminates, which showed a good agreement between the predicted and experimental results.

Voyiadjis and Kattan [10-11], Voyiadjis and Park [12] and Voyiadjis and Deliktas [13] developed a 3-D model for coupled progressive damage and plasticity using a symmetric second order damage tensor. The eigenvectors of this tensor represent the principal directions of damage and the eigenvalues represent the density of the distributed microcracks that are normal to the respective eigenvectors. Kattan and Voyiadjis [14] also used a micromechanical composite approach to study the damage of a uniaxially loaded unidirectional fiber-reinforced composite thin lamina. Their method was based on the concept of effective stress, and overall damage variables. The local damage effects were modeled through two additional separate damage variables, which represent matrix and fiber damages. A relation between tangential modulus and the initial elastic modulus with damage variables were derived from the experimental stress–strain curves due to the uniaxial tensile loading.

Barbero and De Vivo [15] developed a 2D plane stress model for progressive damage based on the use of a symmetric second order damage tensor. Damage evolution and stiffness reduction were computed for the pre-homogenized composite material simplifying the formulation. Their model was extended by Barbero and Lonetti [16] to include plasticity, and further extended by Lonetti *et.al.* [17] to include triaxial or-

1. *Assistant Professor, School of Mech. Eng., Iran Univ. of Sci. and Tech., Tehran, Iran, Email: Bijan_Mohammadi@iust.ac.ir.*
2. *(Corresponding Author), Professor, Dept. of Aerospace Eng., Amirkabir Univ. of Tech. Tehran, Iran, Email: Hosseini@aut.ac.ir.*
3. *Assistant Professor, Dept. of Aerospace Eng., Amirkabir Univ. of Tech., Tehran, Iran.*

thotropic damage in terms of three damage eigenvalues. They used the triaxial damage model in conjunction with the 3D solid finite elements methods.

In this paper, 3D continuum damage mechanics is used for progressive damage analyses of composite laminates under quasi-static, monotonic loading. For this purpose, a finite element program has been developed using an eight-node 2D layered elements including layer-wise plate theory. The numerical examples include damage analysis of a single orthotropic layer under various uniform in-plane and transverse loading conditions, and laminate problems with diffuse damage under simply supported and distributed transverse loading conditions. The effect of numerical modeling parameters on the progressive damage response and global failure are also investigated.

APPLICATION OF CDM IN COMPOSITE LAMINATE

In the Continuum Damage Mechanics, damage variables can be presented through the internal state variables of thermodynamics for irreversible processes in order to describe the effects of damage and its microscopic growth on the macro-mechanical properties of the materials. Using CDM, distributed microscopic damage can be quantified by the use of a damage tensor field that describes the orientation and density of microcracks in the material.

In a homogenized description of damage, the simplest form of the damage tensor that is capable of accurately describing microscopic damage is a symmetric 2^{nd} order tensor ϕ whose principal directions are assumed to coincide with the principal material directions, i.e. orthotropic damage. The i^{th} eigenvalue ϕ_i represents the effective fractional reduction in load carrying area on planes that are perpendicular to the i^{th} principal material direction. Therefore, this type of damage tensor field is capable of quantitatively describing the density and distribution of microscopic cracks that are associated with fiber breakage, fiber/matrix debonding, and matrix cracks that are oriented either parallel to the fibers direction or perpendicular to that as shown in Figure 1. The eigenvalues of the damage tensor are in the range $0 < \phi_i < 1$.

To define stress transformation in a general state of deformation and damage, the effective stress tensor is related to the Cauchy stress tensor by the following linear transformation:

$$\bar{b}\bar{s}\sigma = \mathbf{M}(\boldsymbol{\phi}) : \boldsymbol{\sigma} \tag{1}$$

where $\mathbf{M}$ is a fourth-order linear transformation operator called the damage effect tensor. Depending on the form used for $\mathbf{M}$, it is very clear from Eq. (1) that the effective stress tensor $\bar{\sigma}$ is generally non-symmetric. However, the use of such complicated mechanics can be easily avoided by symmetrizing the effective stress. One of the symmetrization methods given by Cordebois and Sidorof (1979) is used in this study, and is expressed as follows:

$$\bar{\sigma}_{ij} = (\delta_{ik} - \phi_{ik})^{-1/2} \sigma_{kl} (\delta_{jl} - \phi_{jl})^{-1/2} \tag{2}$$

where $\boldsymbol{\delta}$ is the Kronecker delta, and $\boldsymbol{\phi}$ is second-order damage tensor. Corresponding to Eq. (1), the fourth-order damage effect tensor, $\mathbf{M}$, is:

$$M_{ikjl} = (\delta_{ik} - \phi_{ik})^{-1/2} (\delta_{jl} - \phi_{jl})^{-1/2} \tag{3}$$

It is possible to define Hooke's law in the effective fictitious undamaged and damaged state as follows:

$$\bar{\boldsymbol{\sigma}} = \bar{\mathbf{C}}^e : \bar{\boldsymbol{\epsilon}}^e ; \qquad \boldsymbol{\sigma} = \mathbf{C}^e(\boldsymbol{\phi}) : \boldsymbol{\epsilon}^e ; \tag{4}$$

where an over-bar indicates that the quantity is evaluated in the effective configuration and the superscript e denotes quantities. Damaged material stiffness at each step can be expressed in terms of the damage eigenvalues by invoking various strain energy equivalence principles, which states that the elastic energy of the damaged material is in the same form as that of the effective material, which the stress tensor is replaced by the effective stress.

$$\mathbf{C}^e(\boldsymbol{\phi}) = \mathbf{M}^{-1} : \bar{\mathbf{C}}^e : \mathbf{M}^{-T} \tag{5}$$

In Eq. (5), $\bar{\mathbf{C}}^e$ and $\mathbf{C}^e(\boldsymbol{\phi})$ are virgin material stiffness, and damaged stiffness matrix of material respectively.

State laws in the framework of irreversible thermodynamics

In the framework of irreversible thermodynamics, it is possible to decouple the Helmholtz free energy, ψ, into a potential function for each corresponding internal-state variable. Therefore, an analytical expression for the thermodynamic potential can be given as sum of two terms, the strain energy, $E(\boldsymbol{\epsilon}^e, \phi)$, and dissipation energy, $\prod^d(\kappa)$, as follows:

$$\rho\psi = E(\boldsymbol{\epsilon}^e, \boldsymbol{\phi}) + \prod^{d}(\kappa) \tag{6}$$

where κ is overall damage parameter. The strain energy is defined:

$$E(\boldsymbol{\epsilon}^e, \boldsymbol{\phi}) = \frac{1}{2} \boldsymbol{\epsilon}^{eT} : \mathbf{C}^e(\boldsymbol{\phi}) : \boldsymbol{\epsilon}^e \tag{7}$$

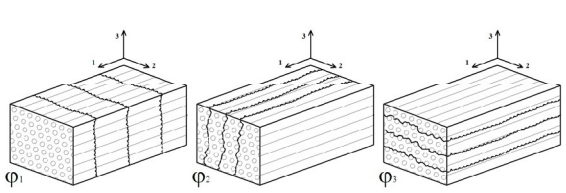

Figure 1. Schematic representation of damage eigenvalues in composites.

In addition, the free energy $\prod^{d}(\kappa)$ introduced to describe the effect of the accumulated damage can be expressed as follows:

$$\prod^{d}(\kappa) = \frac{1}{2}\frac{c_1^d}{c_2^d}\kappa^2 \; or \; \prod^{d}(\kappa) = c_1^d\left[c_2^d \exp\left(\kappa/c_2^d\right) - \kappa\right] \; ; \tag{8}$$

where c_1^d, and c_2^d are the material constants The state laws can be written from the thermodynamic potential equation in the following form

$$\boldsymbol{\sigma} = \rho\frac{\partial\psi}{\partial\boldsymbol{\epsilon}^e} \tag{9}$$

$$\mathbf{Y} = -\frac{\partial\psi}{\partial\boldsymbol{\phi}} \tag{10}$$

$$\mathbf{K} = -\frac{\partial\psi}{\partial\kappa} \tag{11}$$

where $\boldsymbol{\sigma}$, $\mathbf{Y}$, $\mathbf{K}$ are stress tensor, damage conjugate force tensor, and isotropic hardening/softening conjugate relation, respectively. Using these equations, damage potential and damage evolutions can be defined.

Damage condition and evolution equations

Associative damage can be used here to derive the evolution equations for the constitutive model which the damage potential, G, is equal to the damage criterion, g. Analogous to plasticity, it is postulated that damaging behavior can be distinguished from non-damaging behavior on a local basis by a damage surface of the form:

$$G = g\left(\mathrm{Y},\kappa\right) = \sqrt{\mathrm{Y.J.Y}} - \left(K\left(\kappa\right) - K_0\right) \tag{12}$$

where $K(\kappa)$ is damage hardening/softening law, and K_0 is the initial damage threshold at which damage begins to occur. The Y_i are eigenvalues of damage conjugate forces tensor defied in Eq. (3). $g(\mathbf{Y},\kappa) < 0$ indicates a non-damaging state, $g(\mathbf{Y},\kappa) = 0$ indicates a damage inducing state, and $g(\mathbf{Y},\kappa) > 0$ is understood to be inadmissible.

Damage evolution equations can be obtained from dissipation potential function. If the potential function is chosen to define convex surface containing the origin of the forces space, then the satisfaction of the second law of thermodynamics, Clausius-Duhem's inequalities, is be assured in the local form. The energy dissipation due to damage are found by substituting the thermodynamic state laws into the Clausius-Duhem inequality and are thus given as the product of the thermodynamic conjugate forces with the respective flux variables as follows:

$$\prod = \sigma : \dot{\varepsilon}^{id} - \mathrm{Y} : \dot{\varphi} - K\,.\,\dot{\kappa} - \mathrm{q}.\frac{\nabla T}{T} \geq 0 \tag{13}$$

ρ is the mass density, q is the heat flux vector, ΔT is the temperature gradient, and dot over the parameters is the time derivative of parameters. Also, $\boldsymbol{\epsilon}^{id}$ is inelastic-damage part of the strain tensor. Using the theory of functions of several variables, damage Lagrange multiplier $\dot{\lambda}^d$ is utilized to construct the objective function Ω in the following form:

$$\Omega = \prod - G\dot{\lambda}^d \tag{14}$$

where $G = 0$ is the damage potential. In order to obtain the damage tensor rate, and deriving evolution equations for the hardening state variables, the following conditions are used to extremize the objective function:

$$\frac{\partial\Omega}{\partial\boldsymbol{\sigma}} = 0\,; \qquad \frac{\partial\Omega}{\partial\mathbf{Y}} = 0; \qquad \frac{\partial\Omega}{\partial K} = 0; \tag{15}$$

when $G \geq 0$, the corresponding evolution equations for the damage tensor, and the corresponding hardening state variables, are given as follows:

$$\dot{\boldsymbol{\epsilon}}^{id} = +\frac{\partial G}{\partial\boldsymbol{\sigma}}\dot{\lambda}^d\,; \quad \dot{\boldsymbol{\phi}} = -\frac{\partial G}{\partial\mathbf{Y}}\dot{\lambda}^d; \quad \dot{\kappa} = -\frac{\partial G}{\partial K}\dot{\lambda}^d; \tag{16}$$

The following loading–unloading conditions known as the Kuhn–Tucker optimality conditions must also be enforced:

$$\dot{\lambda}^d \geq 0\,; \quad G \leq 0\,; \quad \dot{\lambda}^d G = 0; \tag{17}$$

Stress Integration algorithm

In the solution procedure, a linearized form of the governing equation is solved within an incremental iterative Newton–Raphson solution procedure for the increment of strain over the time increment.

The increments of the damage multiplier, $\Delta\lambda^{d}{}_{j}$, must be computed, and then the state variables are updated using Eq. (16):

$$\begin{aligned}
\boldsymbol{\epsilon}_j^{id} &= \boldsymbol{\epsilon}_c^{id} + \Delta\boldsymbol{\epsilon}_j^{id} \\
\boldsymbol{\phi}_j &= \boldsymbol{\phi}_o + \Delta\boldsymbol{\phi}_j \\
\boldsymbol{\kappa}_j &= \boldsymbol{\kappa}_o + \Delta\boldsymbol{\kappa}_j
\end{aligned} \tag{18}$$

The $\boldsymbol{\sigma}$ and $\mathbf{Y}$ for this integration scheme are defined at j^{th} iteration as follows:

$$\begin{aligned}
\boldsymbol{\sigma}_j = \mathbf{C}^e : \left(\boldsymbol{\epsilon}_j - \boldsymbol{\epsilon}_j^{id}\right) &= \boldsymbol{\sigma}_o + \mathbf{C}_j^e : \left(\Delta\boldsymbol{\epsilon}_j - \Delta\boldsymbol{\epsilon}_j^{id}\right) \\
&+ \mathbf{C}_j^e : \left(\mathbf{C}^{-e} : \frac{\partial\mathbf{C}^e}{\partial\boldsymbol{\phi}} : \left(\boldsymbol{\epsilon} - \boldsymbol{\epsilon}^{id}\right)\right)_j : \Delta\boldsymbol{\phi}_j
\end{aligned} \tag{19}$$

$$\mathbf{Y}_j = \boldsymbol{\sigma}_j^T : \left(\frac{\partial\mathbf{C}^{-e}}{\partial\boldsymbol{\phi}}\right)_j : \boldsymbol{\sigma}_j \tag{20}$$

The integration scheme used here enforces that g_j=0 at the end of the time step:

$$g_j = g(\mathbf{Y}_j, \kappa_j) = \sqrt{\mathbf{Y}_j.\mathbf{J}.\mathbf{Y}_j} - (K(\kappa j) - K_0) = 0 \tag{21}$$

In order to address this type of problem, a return-mapping algorithm is used. This algorithm has an initial elastic-predictor step, followed by a damage-corrector step. In the elastic-predictor step, the incremental strains are assumed to be elastic with no damage increment such that an initial trial stress and an initial trial damage conjugate force can be computed as:

$$\boldsymbol{\sigma}_j^{trial} = \boldsymbol{\sigma}_o + \mathbf{C}_o^e : \Delta\boldsymbol{\epsilon}_j \tag{22}$$

$$\mathbf{Y}_j^{trial} = \boldsymbol{\sigma}_j^{trial} : \left(\frac{\partial \mathbf{C}^{-e}}{\partial \boldsymbol{\phi}}\right)_j : \boldsymbol{\sigma}_j^{trial} \tag{23}$$

The trial state $(\boldsymbol{\sigma}_j^{trial}, \mathbf{Y}_j^{trial}, \boldsymbol{\epsilon}_o^{id}, \boldsymbol{\phi}_o, \kappa_o)$ is then used in a trial damage criterion to decide whether an elastic point enters the damage regimes or whether a damage point elastically unloads. For the case when $g^{trial} < 0$, the integration point is assumed to be elastic with no additional damage and the current state of $(\boldsymbol{\sigma}_j, \mathbf{Y}_j, \boldsymbol{\epsilon}_o^{id}, \boldsymbol{\phi}_o, \kappa_o)$ is equal to the trial state of $(\boldsymbol{\sigma}_j^{trial}, Y_j^{trial}, \boldsymbol{\epsilon}_o^{id}, \boldsymbol{\phi}_o, \kappa_o)$. When $g^{trial} > 0$, the current state resulting from this trial state lies outside of the damage surface. Damage has occurred and the state has to be returned to the damage surface. Using the definition of the Cauchy stress from Eq. (19) along with the definition of the trial stress, Eq. (22), the Cauchy stress is corrected as follows:

$$\Delta\boldsymbol{\sigma}_j = \boldsymbol{\sigma}_j - \boldsymbol{\sigma}_j^{trial} = \Delta\mathbf{C}_j^e : \Delta\boldsymbol{\epsilon}_j - \mathbf{C}_j^e : \Delta\boldsymbol{\epsilon}_j^{id} + \mathbf{C}_j^e : \left(\mathbf{C}^{-e} : \frac{\partial \mathbf{C}^e}{\partial \boldsymbol{\phi}} : (\boldsymbol{\epsilon} - \boldsymbol{\epsilon}^{id})\right)_j : \Delta\boldsymbol{\phi}_j \tag{24}$$

While the trial stress is computed based upon the increment of the total strain, this inelastic corrector is computed based upon the total increments of the damage multiplier, which are computed from the used integration scheme. In this scheme, the increment of the multiplier is set to zero ($\Delta\lambda_j^{d(0)} = 0$), and it is incremented by $d\lambda_j^{d(k)}$ at each iteration, k.

$$\Delta\lambda_j^{d(k+1)} = \Delta\lambda_j^{d(k)} + d\lambda_j^{d(k)} \tag{25}$$

$d\lambda_j^{d(k)}$ can be computed using a linearization form of the nonlinear equation of, $g(\Delta\lambda)$:

$$g^{(k)} + \frac{dg^{(k)}}{d\Delta\lambda_j^{d(k)}} d\lambda_j^{d(k)} = 0 \tag{26}$$

An implicit backward Euler algorithm presented by Belytschko *et.al.* [18] is used for the integration of the constitutive model. The integration scheme is defined by Eq. (16), where the state variables increments are written as follows:

$$\Delta\boldsymbol{\epsilon}_j^{id} = g_{,\boldsymbol{\sigma}_j}\Delta\lambda_j^d$$
$$\Delta\phi_j = -g_{,\mathbf{Y}_j}\Delta\lambda_j^d$$
$$\Delta\kappa_j = -g_{,\kappa_j}\Delta\lambda_j^d \tag{27}$$

The increment of the elastic stiffness tensor is also defined here as follows:

$$\Delta\mathbf{C}_j^e = \left(\frac{\partial \mathbf{C}^e}{\partial \boldsymbol{\phi}}\right)_j : \Delta\boldsymbol{\phi}_j = 2\mathbf{C}_j^e : \mathbf{M}_j^T : \left(\frac{\partial \mathbf{M}^{-T}}{\partial \boldsymbol{\phi}}\right)_j : \Delta\boldsymbol{\phi}_j \tag{28}$$

Thus, correction of the stress during the corrector phase can be written as follows:

$$\Delta\boldsymbol{\sigma}_j = -\mathbf{C}_j^e : \Delta\boldsymbol{\epsilon}_j^{id} + \left(\frac{\partial \mathbf{C}^e}{\partial \varphi}\right)_j : \left(\boldsymbol{\epsilon}_j + \Delta\boldsymbol{\epsilon}_j - \boldsymbol{\epsilon}_j^{id}\right) : \Delta\boldsymbol{\phi}_j \tag{29}$$

It can be seen that the problem defined by this model can be entirely defined by solving for two unknowns, $\Delta\sigma_j$, and $\Delta\lambda^d{}_j$, through the use of the following two nonlinear equations obtained from Eqs. (27) and (21):

$$\tilde{\mathbf{e}}_j - \boldsymbol{\epsilon}_j^{id} + \boldsymbol{\epsilon}_o^{id} + g_{,\boldsymbol{\sigma}_j}\Delta\lambda_j^d = 0 \tag{30}$$

$$g_j = g(\mathbf{Y}_j, \kappa_j) = \sqrt{\mathbf{Y}_j.\mathbf{J}.\mathbf{Y}_j} - (K(\kappa_j) - K_0) = 0 \tag{31}$$

Where $\tilde{\mathbf{e}}_j$ is the residual of the first equation in (27). Using Eq. (26), these equations can be linearized in the same as Eq. (24).

The increments of the unknown stress and the unknown damage multiplier can be derived at k^{th} iteration, and the unknowns are updated as follows:

$$\Delta\lambda_j^{d(k+1)} = \Delta\lambda_j^{d(k)} + d\lambda_j^{d(k)} \tag{32}$$

$$\boldsymbol{\sigma}_j^{(k+1)} = \boldsymbol{\sigma}_j^{(k)} + d\boldsymbol{\sigma}_j^{(k)} \tag{33}$$

Using the increments of the damage multiplier, the increments of the damage surface normals, $dg^{(k)}_{;\boldsymbol{\sigma}_j}$ and $dg^{(k)}_{;\mathbf{Y}_j}$, are computed by the expansion in terms of the increment of the unknowns, and then using the resulting matrices, the state variables are updated as follows:

$$\boldsymbol{\epsilon}_j^{id(k+1)} = \boldsymbol{\epsilon}_j^{id(k)} + \mathbf{g}_{,\boldsymbol{\sigma}_j}^{(k)} d\lambda_j^{d(k)} + d\mathbf{g}_{;\boldsymbol{\sigma}_j}^{(k)} \Delta\lambda_j^{d(k)} \tag{34}$$

$$\phi_j^{(k+1)} = \phi_j^{(k)} - g_{,\mathbf{Y}_j}^{(k)} d\lambda_j^{d(k)} - dg_{,\mathbf{Y}_j}^{(k)} \Delta\lambda_j^{d(k)} \tag{35}$$

$$\kappa_j^{(k+1)} = \kappa_j^{(k)} - g_{,K_j}^{(k)} d\lambda_j^{d(k)} \tag{36}$$

The Newton iteration procedure is repeated until the convergence is obtained by checking the values of e, and g_j from Eqs. (30) and (31) which yields to zero.

In order to obtain proper quadratic convergence, the choice of a tangent operator must be consistent with the integration scheme, which is defined as follows using the purposed procedure by Belytschko [18]:

$$\mathbf{C}_j^{a\,\mathrm{lg}} = \left(\frac{d\boldsymbol{\sigma}}{d\boldsymbol{\epsilon}}\right)_j = \left[\bar{\mathbf{C}}_j^{ed}\right]^{a\,\mathrm{lg}} \tag{37}$$

Where the superscript "alg" denotes the algorithmic calculated consistent tangent stiffness matrix. Equation (37) can be used as a consistent tangent operator to calculate the layer-wise finite element stiffness matrix in a proper form which is explained in the next section.

Layer-wise finite element formulation in conjunction with CDM

Considering a laminated plate composed of N orthotropic lamina, each being arbitrarily oriented with respect to the laminate (x, y) coordinates. The coordinate center is taken to be in the mid-plane of the laminate, z is through the thickness and (x, y) are in-plane coordinates. The displacements (u_1, u_2, u_3) correspond to the (x, y, z) directions at each point in the laminate are assumed to be in the form of:

$$\begin{aligned} u_1(x,y,z) &= u(x,y) + U(x,y,z) \\ u_2(x,y,z) &= v(x,y) + V(x,y,z) \\ u_3(x,y,z) &= w(x,y) \end{aligned} \tag{38}$$

where (u, v, w) are the displacement components of a point $(x, y, 0)$ on the reference plane of the laminate, and U and V are functions which vanish on the reference plane as $U(x, y, 0) = V(x, y, 0) = 0$. Also U and V can be approximated as:

$$\begin{aligned} U(x,y,z) &= \sum_{m=1}^{n} U^m(x,y)\phi^m(z) \\ V(x,y,0) &= \sum_{m=1}^{n} V^m(x,y)\phi^m(z) \end{aligned} \tag{39}$$

where U^m, and V^m are undetermined coefficients, and ϕ^m are any continuous functions that satisfy the condition $\phi^m(0) = 0$ for all $m = 1, 2, \ldots, n$. For example, a finite element approximation based on the Lagrangian interpolation through the thickness can be obtained from Eq. (39) considering the $n = pN + 1$, where N is the number of layers through the thickness, p is the degree of the interpolation polynomials of $\phi^m(z)$. The approximation in Eq. (38) can also be viewed as the global semi-discrete finite element approximations of U and V through the thickness. In that case ϕ^m denote the through thickness interpolation functions, and U^m, and V^m, are the global nodal values of U and V at the nodes through the thickness of the laminate. Note that the transverse deflection here is assumed independent of the thickness coordinate, which leads to neglect the transverse normal stress.

In order to understand the relation between the nodal resultant forces of laminate and displacements in layer-wise plate theory, the first variation of potential energy, equilibrium condition, is expanded as follows:

$$\begin{aligned} \delta\Pi = \frac{1}{2}\int_A \Bigg\{ & N_x\left(\frac{\partial\delta u}{\partial x}\right) + N_y\left(\frac{\partial\delta v}{\partial y}\right) + N_{xy}\left(\frac{\partial\delta u}{\partial y} + \frac{\partial\delta v}{\partial x}\right) \\ & + Q_x\frac{\partial\delta w}{\partial x} + Q_y\frac{\partial\delta w}{\partial y} + \sum_{m=1}^{N}\left[Q_x^m\delta U^m + Q_y^m\delta V^m\right] \\ & + \sum_{m=1}^{N}\Bigg[N_x^m\left(\frac{\partial\delta U^m}{\partial x}\right) + N_y^m\left(\frac{\partial\delta V^m}{\partial y}\right) \\ & + N_{xy}^m\left(\frac{\partial\delta U^m}{\partial y} + \frac{\partial\delta V^m}{\partial x}\right)\Bigg]\Bigg\}\, dA = 0 \end{aligned} \tag{40}$$

where the resultant forces of the laminate are:

$$\begin{aligned} N_x, N_y, N_{xy} &= \int_{-t/2}^{t/2} (\sigma_x, \sigma_y, \sigma_{xy}) dz \\ Q_x, Q_y &= \int_{-t/2}^{t/2} (\sigma_{xz}, \sigma_{yz}) dz \\ N_x^m, N_y^m, N_{xy}^m &= \int_{-t/2}^{t/2} (\sigma_x, \sigma_y, \sigma_{xy})\phi^m(z) dz \\ Q_x^m, Q_y^m &= \int_{-t/2}^{t/2} (\sigma_{xz}, \sigma_{yz})\frac{d\phi^m(z)}{dz} dz \end{aligned} \tag{41}$$

σ_x, σ_y, σ_{xy}, σ_{xz}, and σ_{yz} are the stress components. The constitutive equations of the laminate in damage state are given by:

$$\begin{aligned} \{N\} &= [A]^{(a\,\mathrm{lg})}\{e\} + \sum_{k=1}^{N}[B^m]^{(a\,\mathrm{lg})}\{e^m\} \\ \{N^m\} &= [B^m]^{(a\,\mathrm{lg})}\{e\} + \sum_{k=1}^{N}[D^{mr}]^{(a\,\mathrm{lg})}\{e^m\} \end{aligned} \tag{42}$$

where $\{e\}$ and $\{e^m\}$ are the in-plane and layers interfaces strain vectors respectively, and $[A]^{(a\,\mathrm{lg})}$, $[D^{mr}]^{(a\,\mathrm{lg})}$, and $[B^m]^{(a\,\mathrm{lg})}$ are extensional, bending

stiffness, and bending-extensional coupling stiffness matrices respectively, defined as follows:

$if\,(p,q=1,2,6)$

$$A_{pq}^{(a\,\mathrm{lg})}=\sum_{k=1}^{N}\int_{z_k}^{z_{k+1}}C_{pq}^{(a\,\mathrm{lg})^k}\,dz$$

$$B_{pq}^{(a\,\mathrm{lg})^m}=\sum_{k=1}^{N}\int_{z_k}^{z_{k+1}}C_{pq}^{(a\,\mathrm{lg})^k}\,\phi^m dz$$

$$D_{pq}^{(a\,\mathrm{lg})^{mr}}=\sum_{k=1}^{N}\int_{z_k}^{z_{k+1}}C_{pq}^{(a\,\mathrm{lg})^k}\,\phi^m\phi^r dz \tag{43}$$

$if\,(p,q=4,5)$

$$A_{pq}^{(a\,\mathrm{lg})}=\sum_{k=1}^{N}\int_{z_k}^{z_{k+1}}C_{pq}^{(a\,\mathrm{lg})^k}\,dz$$

$$B_{pq}^{(a\,\mathrm{lg})^m}=\sum_{k=1}^{N}\int_{z_k}^{z_{k+1}}C_{pq}^{(a\,\mathrm{lg})^k}\,\frac{d\phi^m}{dz}dz$$

$$D_{pq}^{(a\,\mathrm{lg})^{mr}}=\sum_{k=1}^{N}\int_{z_k}^{z_{k+1}}C_{pq}^{(a\,\mathrm{lg})^k}\,\frac{d\phi^m}{dz}\frac{d\phi^r}{dz}dz \tag{44}$$

where $C_{pq}^{(a\,\mathrm{lg})}$ is elastic-damage reduced stiffness matrix. In the case of pure elastic behavior, $C_{pq}^{(a\,\mathrm{lg})}$ should be replaced by the elastic stiffness tensor, and Q_{pq} defined in mechanics of composite materials. The local stresses in each constituent can be obtained from the applied loading increment by using the assumption of the lamination theory.

Integration in the thickness direction is performed using linear variation; two points at the top and bottom of each numerical layer are considered for calculation of stiffness properties through the thickness. If the piecewise linear functions through the thickness of the laminate are considered for damage effects, the following explicit relations can be obtained for the coefficients of the laminate stiffness matrices.

<u>$if\ p,q=1,2,4,5,6;$</u>

$$A_{pq}^{(a\,\mathrm{lg})}=\sum_{k=1}^{N}\frac{1}{2}\left({}^{T}C_{pq}^{(a\,\mathrm{lg})^k}+{}^{B}C_{pq}^{(a\,\mathrm{lg})^k}\right)t_L^k$$

<u>$if\ p,q=1,2,6;$</u>

$$B_{pq}^{(a\,\mathrm{lg})^m}=\left(\frac{{}^{T}C_{pq}^{(a\,\mathrm{lg})^{m-1}}}{3}+\frac{{}^{B}C_{pq}^{(a\,\mathrm{lg})^{m-1}}}{6}\right)t_L^{m-1}+\left(\frac{{}^{T}C_{pq}^{(a\,\mathrm{lg})^m}}{6}+\frac{{}^{B}C_{pq}^{(a\,\mathrm{lg})^m}}{3}\right)t_L^m$$

$$D_{pq}^{(a\,\mathrm{lg})^{mm}}=\left(\frac{{}^{T}C_{pq}^{(a\,\mathrm{lg})^{m-1}}}{4}+\frac{{}^{B}C_{pq}^{(a\,\mathrm{lg})^{m-1}}}{12}\right)t_L^{m-1}+\left(\frac{{}^{T}C_{pq}^{(a\,\mathrm{lg})^m}}{12}+\frac{{}^{B}C_{pq}^{(a\,\mathrm{lg})^m}}{4}\right)t_L^m$$

$$D_{pq}^{(a\,\mathrm{lg})^{mr}}=D_{pq}^{(a\,\mathrm{lg})^{rm}}=\left({}^{T}C_{pq}^{(a\,\mathrm{lg})^m}+{}^{B}C_{pq}^{(a\,\mathrm{lg})^m}\right)\frac{t_L^m}{12}$$

<u>$if\ \ p,q=4,5;$</u>

$$B_{pq}^{(a\,\mathrm{lg})^m}=\frac{1}{2}\left({}^{T}C_{pq}^{(a\,\mathrm{lg})^{m-1}}+{}^{B}C_{pq}^{(a\,\mathrm{lg})^{m-1}}\right)-\frac{1}{2}\left({}^{T}C_{pq}^{(a\,\mathrm{lg})^m}+{}^{B}C_{pq}^{(a\,\mathrm{lg})^m}\right)$$

$$D_{pq}^{(a\,\mathrm{lg})^{mm}}=\left(\frac{{}^{T}C_{pq}^{(a\,\mathrm{lg})^{m-1}}+{}^{B}C_{pq}^{(a\,\mathrm{lg})^{m-1}}}{2t_L^{m-1}}\right)+\left(\frac{{}^{T}C_{pq}^{(a\,\mathrm{lg})^m}+{}^{B}C_{pq}^{(a\,\mathrm{lg})^m}}{2t_L^m}\right)$$

$$D_{pq}^{(a\,\mathrm{lg})^{mr}}=D_{pq}^{(a\,\mathrm{lg})^{rm}}=-\left(\frac{{}^{T}C_{pq}^{(a\,\mathrm{lg})^m}+{}^{B}C_{pq}^{(a\,\mathrm{lg})^m}}{t_L^m}\right) \tag{45}$$

where the coefficients are computed in terms of the damage values of the reduced stiffness coefficients in global coordinates and superscripts T and B refer to top and bottom of each layer, respectively.

In the incremental form, the weak form of the equilibrium equation with the elastic-damaged material stiffness matrix at j^{th} time step is as follows:

$$\int_V \delta\boldsymbol{\epsilon}:\mathbf{C}_j^{ed}:d\boldsymbol{\epsilon}_j dV=-\int_v \delta\mathbf{u}:\mathbf{b}_j dV-\int_{\Gamma_t}\delta\mathbf{u}:\hat{\mathbf{t}}_j d\Gamma-\int_V \delta\boldsymbol{\epsilon}:\boldsymbol{\sigma}_j dV \tag{46}$$

where ϵ, $\mathbf{C}^{ed}$, $\boldsymbol{\sigma}$, $\mathbf{u}$, $\mathbf{b}$, $\hat{\mathbf{t}}$, and V are strain vector, material stiffness matrix, stress vector, displacement vector, body inertia force vector, traction external force vector, and total volume of body respectively Note that this equation is enforced over the entire body, including both the damage and elastic domains. In the right hand side of the governing equations, the stress at j^{th} iteration must be known. It was explained in the integration scheme, that for each integration point in an inelastic state, the implicit backward Euler elastic predictor-inelastic corrector algorithm is used to compute the stress. The governing equation can be linearized consistently and solved within an incremental iterative Newton-Raphson solution procedure.

The displacement filed, u_j, is discretized using layer-wise plate theory. The interpolating relation is

defined as follows:

$$\mathbf{u}_j = [\psi] \left\{ \begin{array}{c} \Delta \\ \Delta^m \end{array} \right\}_j ; \quad \{\Delta\} = \left\{ \begin{array}{c} \mathbf{u} \\ \mathbf{v} \\ \mathbf{w} \end{array} \right\} ;$$

$$\{\Delta^m\} = \left\{ \begin{array}{c} \mathbf{U}^m \\ \mathbf{V}^m \end{array} \right\} ; \quad [\psi] = \left[\begin{array}{cc} [\mathbf{N}] & 0 \\ 0 & [\phi^m] \end{array} \right] \tag{47}$$

where $[\mathbf{N}]$ and $[\phi^m]$ contains the in-plane and through the thickness set of nodal elements of the well-known finite element shape functions, respectively. Also (u, v, w) and (U^m, V^m) are mid-plane and numerical layers nodal displacements, respectively. By taking the required derivatives, the strains are obtained using the following strain-displacement relation:

$$\epsilon_j = [\mathbf{B}] \{\mathbf{u}\}_j$$

$$\epsilon_j = \left\{ \begin{array}{c} \mathbf{e}_j \\ \mathbf{e}_j^m \end{array} \right\} ; \ \mathbf{e}_j = [\mathbf{B_L}] \{\Delta\} ; \ \mathbf{e}_j^m = \left[\bar{\mathbf{B}}_\mathbf{L}\right] \{\Delta^m\} \tag{48}$$

$$[\mathbf{B}] = \left[\begin{array}{cc} [\mathbf{B_L}] & 0 \\ 0 & [\bar{\mathbf{B}}_\mathbf{L}] \end{array} \right] \tag{49}$$

where $[\mathbf{B}_L]$ and $[\bar{\mathbf{B}}]$ are matrices of shape function derivatives of mid-plane and numerical layers degree of freedom respectively. Using this discretization, the weak form of the equilibrium equation becomes:

$$\begin{aligned} &\{\delta \mathrm{u}\}_j^T \int_{\Gamma_t} [\mathrm{B}]^T \left[\mathrm{E}^{ed}\right]_j^{a\,\mathrm{lg}} [\mathrm{B}] \{du\}\, d\Gamma \\ &= \{\delta \mathrm{u}\}_j^T \left(\int_V [\psi]^T \{\mathrm{b}\}_j \, dV \right. \\ &\left. + \int_{\Gamma_t} [\psi]^T \{\hat{\mathrm{t}}\}_j \, d\Gamma - \int_V [\mathrm{B}]^T \{\sigma\}_j \right) dV \end{aligned} \tag{50}$$

where $\left[E^{ed}\right]_j^{(a\,\mathrm{lg})}$ is:

$$\left[\mathrm{E}^{ed}\right]_j^{(a\,\mathrm{lg})} = \left[\begin{array}{cc} [\mathrm{A}]_j^{(a\,\mathrm{lg})} & [\mathrm{B}^m]_j^{(a\,\mathrm{lg})} \\ [\mathrm{B}^m]_j^{(a\,\mathrm{lg})} & [\mathrm{D}^{mr}]_j^{(a\,\mathrm{lg})} \end{array} \right] \tag{51}$$

It is noted that transpose of matrix $[\mathbf{B}]^T$ is specially defined as follows:

$$[\mathrm{B}]^T = \left[\begin{array}{cc} [\mathrm{B_L}]^T & 0 \\ 0 & [\bar{\mathrm{B}}_\mathrm{L}]^T \end{array} \right] \tag{52}$$

This governing equation must be admissible for any displacement variation, which can be written as a set of algebraic equations:

$$[K]^{ed} \{du\}_j = \{f^{ext}\} + \{f^{\mathrm{int}}\} + \{f^b\} \tag{53}$$

where the sub-matrices are defined as follows:

$$[K]^{ed} = \int_{\Gamma_t} [B]^T \left[E^{ed}\right]_j^{a\,\mathrm{lg}} [B]\, d\Gamma \tag{54}$$

$$\{f^{ext}\} = \int_{\Gamma_t} [\psi]^T \{\hat{t}\}_j \, d\Gamma \tag{55}$$

$$\{f^b\} = \int_V [\psi]^T \{b\}_j \, dV \tag{56}$$

$$\{f^{\mathrm{int}}\} = -\int_V [B]^T \{\sigma\}_j \, dV \tag{57}$$

Using layer-wise lamination theory and finite element procedure, the stiffness matrix and its sub-matrices are obtained:

$$[K]^{ed} = \left[\begin{array}{cccc} [k^{11}] & [k_1^{12}] & \ldots & [k_N^{12}] \\ [k_1^{11}] & [k_{11}^{22}] & \ldots & [k_{1N}^{22}] \\ . & . & \ldots & . \\ [k_N^{21}] & [k_{N1}^{22}] & \ldots & [k_{NN}^{22}] \end{array} \right] \tag{58}$$

where the sub-matrices $[k^{11}]$, $[k_m^{12}]$, $[k_m^{21}]$, and $[k_{mr}^{22}]$ are as follows:

$$\begin{aligned} \left[K^{11}\right] &= \textstyle\sum_e \int_{\Gamma e} \left([B_L]^T [A]^{(a\,\mathrm{lg})} [B_L]\right) d\Gamma_e \\ \left[K_m^{12}\right] &= \textstyle\sum_e \int_{\Gamma e} \left([B_L]^T [B^m]^{(a\,\mathrm{lg})} [\bar{B}_L]\right) d\Gamma_e \\ \left[K_m^{21}\right] &= \textstyle\sum_e \int_{\Gamma e} \left([\bar{B}_L]^T [B^m]^{(a\,\mathrm{lg})} [B_L]\right) d\Gamma_e \\ \left[K_{mr}^{22}\right] &= \textstyle\sum_e \int_{\Gamma e} \left([\bar{B}_L]^T [D^{mr}]^{(a\,\mathrm{lg})} [\bar{B}_L]\right) d\Gamma_e \\ m, r &= 1, 2, 3, \ldots, N \end{aligned} \tag{59}$$

These matrices and vectors can be computed for the elements and then implemented into the global matrices and vectors for the entire body.

Nonlinear solution procedure

The stiffness matrices and load vectors can be computed for each element and then implemented into the global matrices and vectors for the entire body. A finite element procedure is then followed to solve the equations. The problem defined by these equations is nonlinear as the stiffness and the residual loads depend on the deformations. An iterative procedure is required to solve the problem. The nodal forces are produced by the stress field that satisfies the elasto-damage conditions. The difference between these forces and the applied ones gives the residual forces. During a load increment, an element or part of that may prone to damage. All stresses and strains quantities are calculated and monitored at each Gaussian integration

point and therefore the damage occurrence can be determined at such points. Consequently, an element may have partially elastic and partially damage behavior. For any load increment, it is necessary to determine which portion of that is in elastic condition and which part is in damage condition. Then the stress and strain terms are adjusted until satisfaction of the damage criterion. It is noted that the layer-wise element uses a reduced constitutive matrix that is stored as a full 6×6 matrix where its transverse normal stress is zero; therefore, the layer-wise element can directly utilize the full 3D damage mechanics equations in the original form.

For more understanding of the solution procedure, the main steps of the developed computer program to analyze the elastic-damage behavior of the laminates are explained as follows:

1. Defining the problem parameters such as geometry, boundary conditions, loading conditions, load increments functions, material stiffness and strength properties, mesh parameters, and etc.
2. Imposing the jth load increment.
3. Setting the $\Delta\lambda_j^{d(0)} = 0$; $\epsilon_j^{id(0)} = \epsilon_{j-1}^{id}$; $\phi_j^{(0)} = \phi_{j-1}$; $\kappa_j^{(0)} = \kappa_{j-1}$ Compute the algorithmic consistent tangent stiffness matrix of each gauss points using the explained procedure in the previous sections.
4. Compute the element stiffness matrix of each element by considering the step (4) and constructing spars global stiffness matrix.
5. Solving the linearized Eq. (53) and obtaining the displacement field increment.
6. Computing the strains and stresses according to the current load increment at each gauss point in local lamina material coordinate system, and accumulating with the previous converged strain-stress fields.
7. Checking the damage condition. If damage occurs then perform the damage corrector using the explained fully implicit backward Euler return-mapping algorithm.
8. Updating the state variables such as $\Delta\lambda_j^d$, σ_j, ϵ_j^{id}, ϕ_j, κ_j
9. Computing the nodal internal forces of each element by the last updated stress and calculating residual forces at each gauss point.
10. Checking the force and displacement convergence criteria of the overall problem. If they are satisfied, go to the next loading increment; otherwise replace the residual forces in initial incremental load of this step and go to the next overall iteration in step (4).

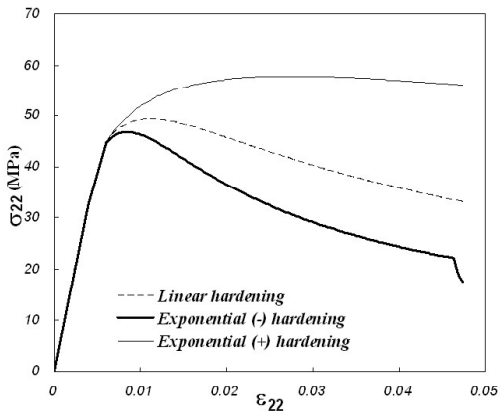

(a)

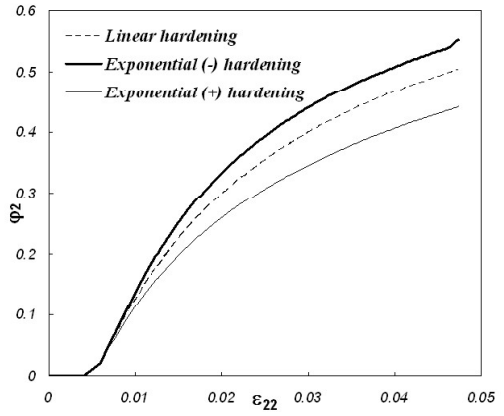

(b)

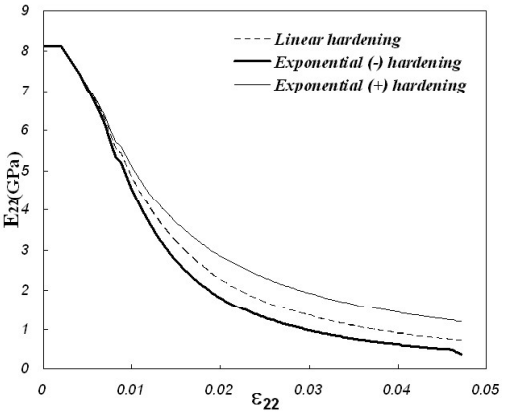

(c)

Figure 2. Progressive damage of a composite ply under pure uniaxial extension in direction '2' (a) stress-strain curve (b) φ_2 versus applied ϵ_{22} (c) in-plane transverse modulus verses applied ϵ_{22}.

11. Repeating the step (2) to step (11) until the total load is applied and all state variables return to the damage surface.

Numerical examples

In this section, numerical examples are performed to discuss the results obtained from the developed program and procedures. To illustrate the basic progressive damage behavior of the present model, a single composite material ply subjected to various modes of imposed homogeneous deformation, resulting in a homogeneous stress state is considered.

In addition, the progressive damage of a simply supported cross-ply laminate under uniform distributed transverse loading is also considered. This problem is chosen since it exhibits diffuse, widespread damage that is driven in different regions by qualitatively different types of combined deformation modes, each of which has different inducing damage characteristics. The used elastic constants for the un-damaged composite material (Graphite/Epoxy) are: E_{11}=167GPa, E_{22}=E_{33}=8.13 GPa, ν_{12}=ν_{13}=ν_{23}=0.27, and G_{12} = G_{13}=G_{23}=8.8252 GPa. Damage surface and hardening constants using Barbero *et.al.* approach [15] are J_{11}= 0.9524e-15; J_{22}= J_{33}= 0.4381e-12.; and the initial damage threshold of $K_o \cong 0.15$ is used.

The behavior of this orthotropic material in fiber direction is 20.5 times stiffer than the either of the transverse directions. Furthermore, the damage surface constants are characterized by J_{11}/J_{22}=J_{11}/J_{33}=0.0022 which is an indicative of orthotropic material exhibiting easily and more damage in the directions of '2' and '3' with respect to '1' (fiber direction). Therefore, under general loading, this particular material is much more likely to exhibit damage in the form of ϕ_2 and/or ϕ_3.

PROGRESSIVE DAMAGE OF COMPOSITE PLIES

Four different modes of homogeneous deformation are chosen to examine the potential causes for specific forms of damage that are commonly observed in laminated composites. Specifically, the following four modes are examined:

Case 1 Uniaxial extension in the direction '2' (causes damage growth of ϕ_2),

Case 2 In-plane shear deformation, (causes damage growth of ϕ_2),

Case 3 Longitudinal shear deformation in the '1-3' plane (causes damage growth of ϕ_3),

Case 4 Transverse shear deformation in the '2-3' plane (causes damage growth of ϕ_2 and ϕ_3).

It is noted that, with an increase in the micro-damage density, there begins to be more interactions between the micro-cracks and between the micro-voids such that damage increase becomes more difficult and the stress required producing additional micro-damage increases. The material exhibits hardening due to the arresting of micro-cracks because of their respective interactions.

To show the influence of the damage hardening rule on the progressive damage behavior, each of the four load cases are solved using three different types of damage hardening rules. All damage-hardening rules have the same initial slope of 7.595e-7 and hence the same initial rate of damage hardening; however, the used three rules show significant differences in the rate of damage hardening after the beginning of damage accumulation.

Linear hardening:

$$K(\kappa) = -\frac{c_1^d}{c_2^d}\kappa; \quad -\frac{c_1^d}{c_2^d} = 7.595e-7$$

Exponential hardening:

$$K(\kappa) = -c_1^d\left[1-\exp\left(\kappa/c_2^d\right)\right];$$

$$\begin{cases}(-) & c_1^d = 0.3; \quad c_2^d = -395000\\ (+) & c_1^d = -0.3; \quad c_2^d = 395000\end{cases}$$

Case 1. Uniaxial Extension in Direction '2'

In this case, nodal displacements are imposed to ensure a uniform distribution of ϵ_2>0, while allows the single ply to freely contract in direction '1' in accordance with the Poisson ratio effect. The maximum imposed node displacement is sufficient to provide an in-plane normal strain of ϵ_2=0.05, and are applied in a series of 200 non-equal load increments. For this particular mode of deformation, ϕ_2 is the only damage eigenvalue that exhibits damage growth.

Parts (a), (b), and (c) of Figure 2 show the axial stress σ_{22}, the damage eigenvalue ϕ_2, and the damaged modulus E_{22} versus the imposed axial strain, ϵ_{22}, respectively. This figure shows that, the type of damage hardening rule have a significant influence on the progressive damage behavior exhibited by the composite material. Since all three damage hardening rules have the same initial slope, they produce similar damage progression at low strain levels (*e.g.*, 0<ϵ_{22}<0.007); however, at larger strain levels (*e.g.*, ϵ_{22}>0.007), the damage behavior is dramatically changed. Figure 2(a) show that, the maximum stress of, σ_2, is strongly dependent on the type of the used damage-hardening rule. Figure 2(b) indicates that, for the imposed strains of larger than, ϵ_{22} = 0.007, the rate of damage growth is strongly dependent on the type of damage hardening rule. Finally, Figure 2(c) shows that, the damaged

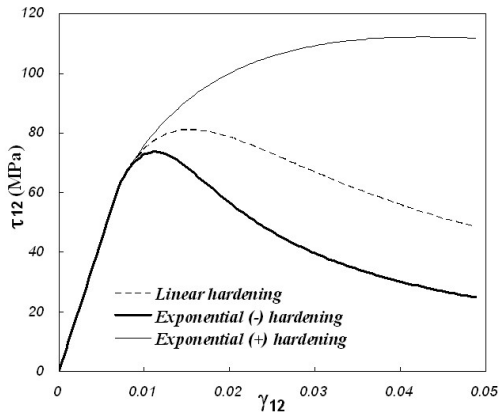

(a)

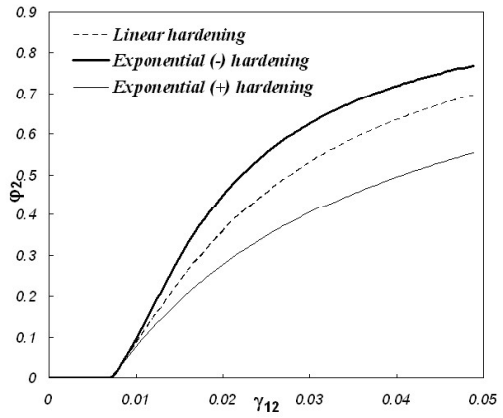

(b)

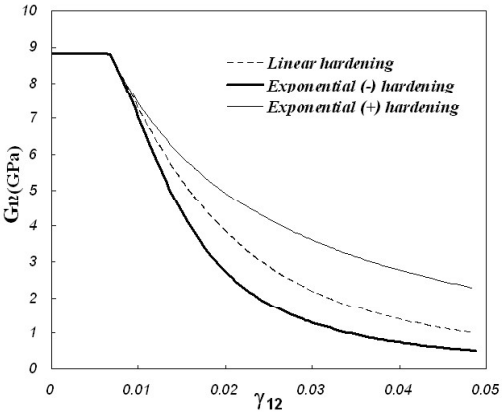

(c)

Figure 3. Progressive damage of a composite ply under imposed homogeneous in-plane shear deformation (a) in-plane shear stress-strain curve (b) ϕ_2 versus applied γ_{12} (c) in-plane shear modulus verses applied γ_{12}.

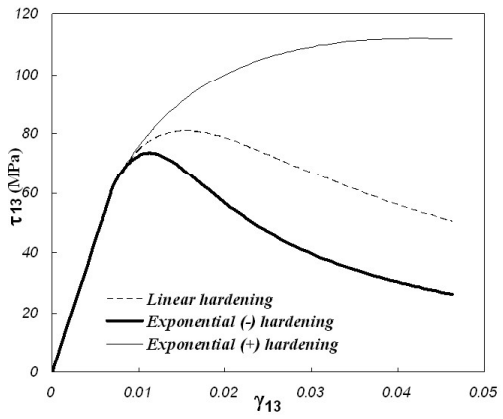

(a)

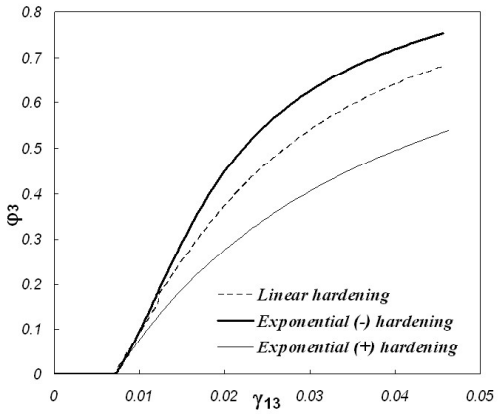

(b)

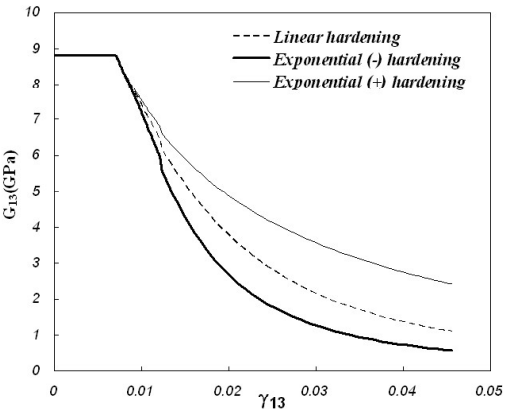

(c)

Figure 4. Progressive damage of a composite ply under imposed homogeneous transverse shear deformation at plane 1-3: (a) transverse shear stress-strain curve (b) ϕ_3 versus applied γ_{13} (c) transverse shear modulus verses applied γ_{13}.

axial modulus of elasticity is also strongly dependent on the type of damage hardening rule. For example, at an imposed strain of ϵ_{22}=0.015, the damaged axial modulus, E_{22}, may be changed by the order of 30% to 45% of the original undamaged modulus value, depending upon the particular used damage hardening rule. Note that the use of a displacement-controlled uniaxial test allows damage progression to be simulated

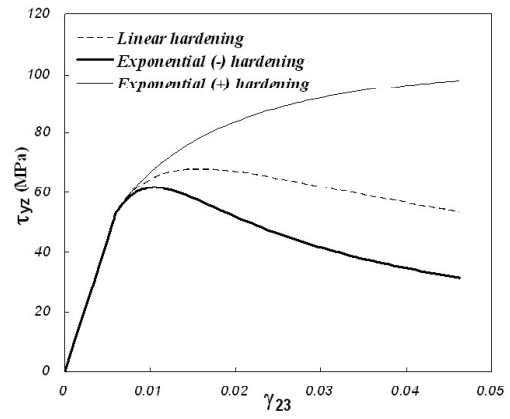

(a)

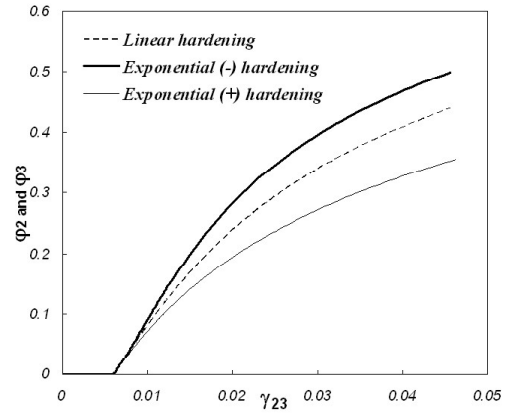

(b)

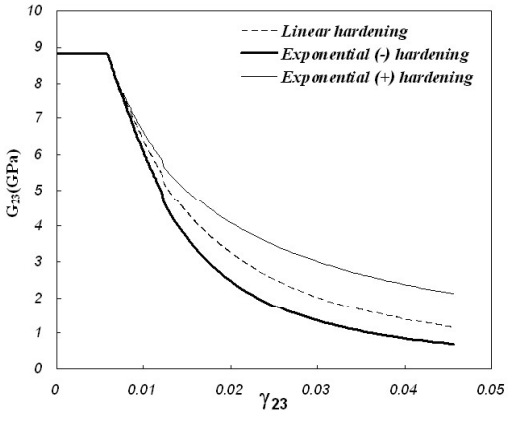

(c)

Figure 5. Progressive damage of a composite ply under imposed homogeneous transverse shear deformation at plane 2-3; (a) transverse shear stress-strain curve (b) ϕ_2 and ϕ_3 versus applied γ_{23} (c) transverse shear modulus verses applied γ_{23}.

to very high levels as seen in Figure 2. A similar force-controlled uniaxial test would simply results in a global material failure (*i.e.*, ϕ_2=1 throughout the single ply) as soon as the imposed axial stress σ_{22} exceeded the maximum values shown in Figure 2(a). The displacement-controlled test was chosen here since it permits the full range of damage behavior to be observed; however, in most of the practical problems, the loading tends to be characterized more as force-controlled rather than displacement controlled.

Case 2. In-Plane Shear Deformation

In this case, nodal displacements are imposed to ensure a uniform distribution of γ_{12}, while all other strain components remain zero. The maximum imposed displacement is sufficient to provide a transverse shear strain of γ_{12}=0.05. This particular mode of deformation produces the growth damage of both ϕ_1 and ϕ_2. However, since the damage surface coefficients are characterized by J_{22}>>J_{11}, the magnitude order growth of ϕ_2 is larger than ϕ_1; hence ϕ_2 exhibits appreciable damage accumulation. Figure 3(a), (b), and (c) show the variations of in-plane shear stress τ_{12}, the damage eigenvalue ϕ_2, and the damaged in-plane shear modulus respectively versus the applied in-plane shear strain γ_{12}. Similar to the extension loading condition explained in Case 1, differences in the progressive damage behavior caused by the three types of damage hardening rules are clearly evident for strains γ_{13}>0.009.

Case 3. Longitudinal Shear Deformation in the '1-3' Plane

In this case, the maximum imposed displacement is sufficient to provide a transverse shear strain of γ_{13}=0.05. This particular mode of deformation produces the damage growth of both ϕ_1 and ϕ_3; however, since the damage surface coefficients are characterized by J_{33}>>J_{11}, the rate of growth of ϕ_3 is larger than ϕ_1; hence ϕ_3 exhibits appreciable accumulation. Figure 4(a), (b), and (c) show the transverse shear stress τ_{13}, the damage eigenvalue ϕ_3, and the damaged shear modulus versus the imposed transverse shear strain, γ_{13} respectively. Once again, differences in the progressive damage behavior caused by the three types of damage hardening rues are evident for strains γ_{13}>0.009.

Case 4. Transverse Shear Deformation in the '2-3' Plane

In this case, the maximum imposed displacement is sufficient to provide a transverse shear strain of γ_{23}=0.05. This particular mode of deformation produces damage growth of both ϕ_2 and ϕ_3. Furthermore, since the damage surface coefficients are characterized by $J_{22} = J_{33}$, both ϕ_2 and ϕ_3 damages exhibit the same rate of growth. Figure 5 (a), (b), and (c) show the transverse shear stress τ_{yz}, the damage eigenvalues ϕ_2 and ϕ_3, and the damaged shear modulus versus the imposed transverse shear strain γ_{23} respectively. Once again,

differences in the progressive damage behavior caused by the three different types of damage hardening rules are evident for strains γ_{13}>0.008. The maximum stress that can be achieved in the material depends heavily upon the type of the used damage-hardening rule.

Case 3 and Case 4 were subjected to the transverse shear deformations of γ_{13} and γ_{23} respectively. In Case 3, the energy dissipation manifests in a single mode of damage (*i.e.*, ϕ_3), while in Case 4, the energy dissipation is divided equally between the two modes of damage (ϕ_2 and ϕ_3). Therefore, it is not surprising that the damage growth rate of φ_3 in Case 3 is higher than the growth rate of ϕ_2 or ϕ_3 in Case 4. Furthermore, the difference between faster growths of a single damage mode versus slower growth of two damage modes causes differences in the transverse shear stress response and the damaged transverse shear moduli.

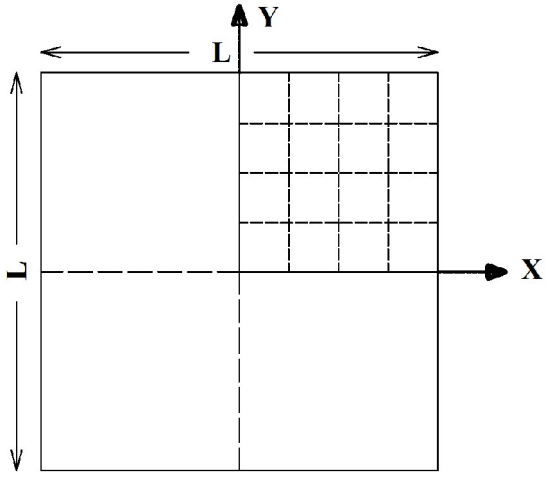

(a)

Computational Domain: 0<x<L/2 ; 0<y<L/2 ; -t/2<z<t/2

Boundary Condition:

w(x,L/2,z)=w(L/2,y,z)=0

u(0,y,z)=u(x,L/2,z)=0 ; v(x,0,z)=v(L/2,y,z)=0

Loading: Transverse Pressure

$q(x,y,t/2)=q_0$

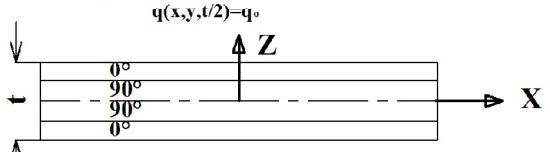

Mesh Type :	In-plane	Thickness direction
EL4-T1=	4×4	1 per material layer
EL4-T2=	4×4	2 per material layer
EL4-T3=	4×4	3 per material layer
EL8-T1=	8×8	1 per material layer
EL8-T2=	8×8	2 per material layer
EL8-T3=	8×8	3 per material layer

(b)

Figure 6. Typical geometry, computational domain and boundary conditions of a simply supported cross-ply laminate.

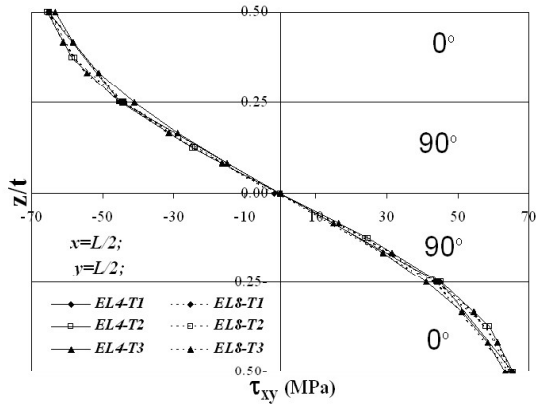

(a)

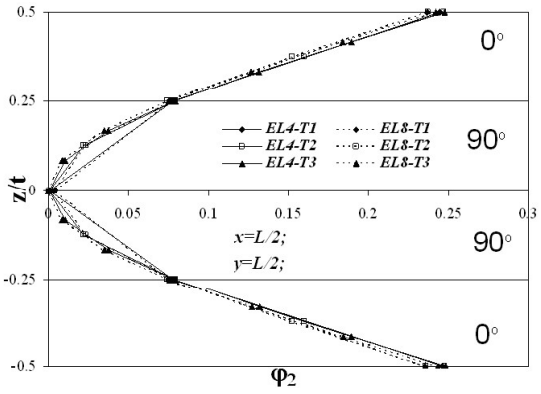

(b)

Figure 7. Distributions of τ_{xy}, and transverse damage eigenvalue at $(x = L/2, y = L/2)$ through the thickness.

PROGRESSIVE DAMAGE AND GLOBAL FAILURE OF A SIMPLY SUPPORTED LAMINATE

We first consider the progressive damage of a simply supported, square, (0/90/90/0) cross-ply laminate subjected to a uniform distributed transverse pressure. Figure 6 shows the geometry and boundary conditions for the simply supported laminate. The boundary conditions are defined for the computational domain is reduced to a quadrant of the laminate via symmetry conditions that exist on the two planes defined by $x = 0$ and $y = 0$. The span to thickness ratio of the laminate is chosen to be $L/t = 10$ in order to ensure that the transverse shear effects play a significant role in the stress field of the laminate. For this example problem, the fiber-reinforced composite material used for each of the four plies is described by the following set of homogenized material coefficients.

A uniform transverse load is imposed by $q(x, y, t/2) = q_0$ on the mid-plane of the laminate in the z-direction. In the solution procedure, the magnitude of the uniform distributed transverse load is

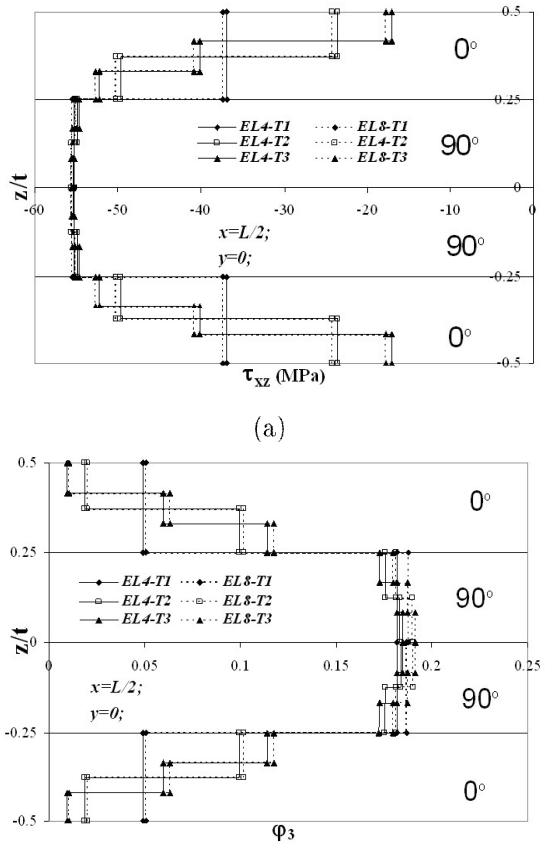

Figure 8. Distributions of τ_{xz}, and thickness direction damage eigenvalue at $(x = L/2, y = L/2)$ through the thickness.

increased until the global failure occurs. The objective to perform this example is to investigate the effects of transverse discretization level and 2-D mesh density on the predicted local damage eigenvalues, and global failure load of the laminate. The effect of in-plane mesh density is investigated using uniform 4×4 and 8×8 meshes of 2-D 8-node quadratic quadrilateral elements with one, two or three discretizations through the thickness of each material layers.

Figure 7 shows distributions of τ_{xy}, and ϕ_2 (damage eigenvalue) through the thickness of the laminate at $x = L/2, y = L/2$. It is known that the in-plane stresses of σ_{yy}, and τ_{xy} have more affects on ϕ_2. At a considered point, σ_{yy} can be neglected rather than τ_{xy}. Considering the bending nature of the loading, it is expected that, the in-plane stresses are increased by increasing the distance from the mid-plane and the in-plane damage eigenvalues are also increased. These facts can also be seen from the results obtained for this example in Figure 8. This figure also shows that there are not considerable differences between the results obtained for the in-plane stresses and damage eigenvalue with various discretizations through the thickness and various in-plane meshes. Therefore, even using a 4×4 mesh may lead to the acceptable results.

Distributions of τ_{xz} and damage eigenvalue, ϕ_3, at $(x = L/2, y = 0)$ through the thickness of the laminate are shown in Figure 8. It is noted that the ϕ_3 parameter depends on the out of plane shear stresses, τ_{xz} and τ_{yz}. Figure 8 also shows that the behavior of ϕ_3 is similar to the behavior of τ_{xz} and it has a maximum value at the mid-plane. This figure also shows that various in-plane mesh densities have not considerable effects on the obtained results. In contrast, dividing the materials layers through the thickness has significant effects on the obtained results, especially on the outer material layers (layers close to the laminate free surfaces). By increasing the thickness discritization, the obtained τ_{xz}, and the corresponding damage eigenvalue, ϕ_3, tend to zero at the laminate free surfaces. It is noted that the values of ϕ_2 had almost the same values of ϕ_3 at the mid-plane surface (except at the corners). Therefore, it can be predicted that, if the uniform applied pressure is increased, delamination type damage may occur at the mid-plane surface of this laminate. Figure 9 shows the variation of damage eigenvalues versus the applied transverse pressure at $(x = L/2, y = 0.0, z = 0.0)$ and $(x = L/2, y = L/2, z = t/2)$. The trend of increasing the ϕ_2 values at the corner doesn't show a damage condition in the applied pressure range. However, the trend of increasing the ϕ_2 and ϕ_3 at $(x = L/2, y = 0.0, z = 0.0)$ which ϕ_2 and ϕ_3 have almost the same values show that the damage eigenvalues tend to unity and therefore damage may occur at this point earlier than the corners.

Table 1 shows the predicted global failure loads of laminates with various transverse discretization and 2-D mesh density. Resolution of the peak transverse shear strain value can affect a progressive damage analysis of fiber-reinforced composite materials. These materials tend to be relatively weak in transverse shear; consequently, the rate of local damage accumulation is quite sensitive to the local magnitude of the transverse shear strain. On the coarse 4×4 2-D mesh, with one division per each material layer predicts a global failure load that is almost 8% higher than that predicted by the most refined model (4×4 2-D mesh with 3 divisions per each material layer). Thus, it can be concluded that by increasing the transverse discretization the

Table 1. Effect of 2-D mesh density and transverse discretization of material layers on global failure load, q_0 (MPa), for a simply supported [0/90]s laminate.

Thickness Discretization	2D Mesh density	
	4×4	8×8
1 div. per Mat. Layer	q_0=14.12	q_0=14.07
2 div. per Mat. Layer	q_0=13.4	q_0=13.325
3 div. per Mat. Layer	q_0=13.175	q_0=13.125

predicted global failure load is decreased. In addition, the differences between the predicted global failure loads with 2 and 3 division per each material layer is about 4 times smaller than the differences obtained with 1 to 2 division per material layer, indicating the numerical convergence by increasing the number of divisions per material layer. It is noted that the global failure load is slightly decreased as the 2-D mesh density increases.

TENSION TEST LAMINATES

In this section, elastic-damage analyses are performed for four different symmetric angle-ply laminates specimens including free edge effects. The obtained results are compared with the available experimental results to validate the developed procedure and code based on the CDM theory. For this purpose three angle-ply lay-ups of [10/-10]2s, [30/-30]2s, [45/-45]2s and a quasi-isotropic lay-up of [0/45/-45/90]s made of T300/5208 graphite-epoxy are considered.

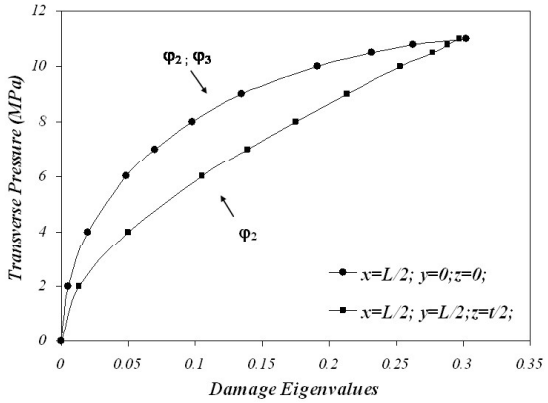

Figure 9. The damage eigenvalues versus the applied transverse pressure at $(x = L/2, y = 0.0, z = 0.0)$ and $(x = L/2, y = L/2, z = t/2)$.

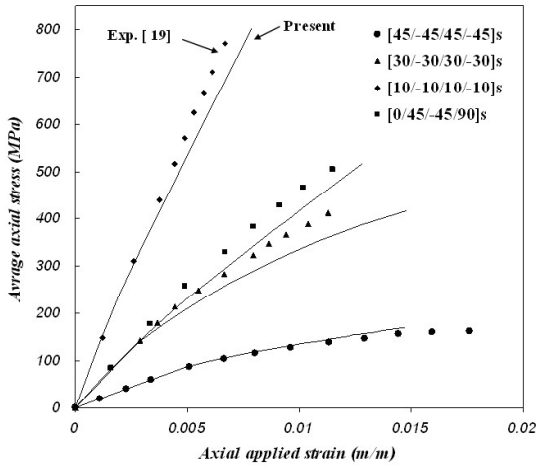

Figure 10. Elastic-damage and experimental average axial stress versus applied axial strain for various lay-ups.

The following homogenized material coefficients are also used for the fiber-reinforced composite material. Elastic constants for the un-damaged T300/5208 [19] are E_{11} = 137.11 GPa; E_{22} = E_{33} = 9.58 GPa; ν_{12}=ν_{13}= ν_{23}=0.28; and G_{12}=G_{13}=G_{23}=4.48 GPa. The damage surface and hardening constants using Barbero *et.al.* approach [25] are also J_{11}= 0.1557320185e-14; J_{22}= 0.5066112225e-13; J_{33}=0.1676262159e-13;c_1^d, and c_2^d.

The obtained average axial stress versus applied axial strain from the elastic-damage analyses are compared with the experimental results [19] for various lay-ups in Figure 10. It is worth to note that the CDM analyses were performed up to the almost the same stress level of experimental failure point for each specimen. This figure shows a good agreement between the obtained responses from CDM analyses and experimental results. The more accurate prediction of the results for the shear stress dominant lay-up of [45/-45]2s may be due to the obtained material characterization for damage initiation and hardening from the pure in-plane shear tests in [25]. For the other lay-ups such as [10/-10]2s and [30/-30]2s the dominant damage mechanism near the final failure is delamination. Therefore, for more accurate prediction of the overall responses and final failure of these lay-ups, the material characterization of thin interface layers between each two layers of the laminates have to be performed and implemented in to the CDM analyses.

CONCLUSIONS

Continuum damage mechanics was implemented to the laminated composites using finite element method including layered 2D elements with layer-wise plate theory. Initiation and propagation of various damage mechanisms in composite laminates can be predicted using the developed procedure.

The resulting layer-wise finite element model was shown to be stable and efficient for the simulation of progressive damage in composite laminates. It was shown that using different types of damage hardening rules may lead to considerable differences in the progressive damage behavior of the laminates. For the simply supported laminate subjected to a uniform distributed transverse load, it was shown that there are not considerable differences between the results obtained for the in-plane stresses and damage eigenvalue with various discretizations through the thickness and various in-plane meshes. In addition, various in-plane mesh densities have not considerable effects on the obtained results. In contrast, dividing the materials layers through the thickness has significant effects on

the obtained results, especially on the outer material layers. It was shown that there is a good agreement between the obtained average axial stress versus applied axial strain responses from CDM analyses and experimental results for various laminates.

REFERENCES

1. Kachanov L.M., "On the Creep Fracture Time", *Zzu. Akad. Nauk. USSR Otd. Tekh.*, (in Russian), **8**, PP 26-31(1958).
2. Lemaitre J., "A Continuous Damage Mechanics Model for Ductile Fracture", *J. Enqnq Mater. Technol.*, **107**, PP 83-89(1985).
3. Lemaitre J., "Local Approach of Fracture", *Enqnq Fract. Mech.*, **25**(5/6), PP 523-537(1986).
4. Chaboche J.L., "Continuum Damage Mechanics. Part I: General Concepts", *J. Appl. Mech.*, **55**, PP 59-64(1988).
5. Chaboche J.L., "Continuum Damage Mechanics. Part II: Damage Growth, Crack Initiation and Crack Grcwth", *J. Appl. Mech.*, **55**, PP 65-72(1988).
6. Krajcinovic D., "Constitutive Equations for Damaging Materials", *J. Appl. Mech.*, **50**, (1983).
7. Krajcinovic D., "Continuum Damage Mechanics", *Appl. Me & Rev.*, **37**(1), PP 1-6(1984).
8. Talreja R., "A Continuum Mechanics Characterization of Damage in Composite Materials", *Proc. R. Soc. A399*, PP 195-216(1985).
9. Talreja R., "Stiffness Properties of Composite Laminates with Matrix Cracking and Interior Delamination", *Eng. Fract. Mech.*, **25**(5/6), PP 151-762(1986).
10. Voyiadjis G.Z., Kattan P.I., "Damage of Fiber Reinforced Composite Mmaterials with Micromechanical Characterization", *Int. J. Solids Struct.*, **30**, PP 2757-2778(1993).
11. Voyiadjis G.Z., Kattan P.I., "Advances in Damage Mechanics: Metals and Metal Matrix Composites", *Elsevier, Amsterdam*, (1999).
12. Voyiadjis G.Z., Park T., "Kinematics Description of Damage for Finite Strain Plasticity", *J. Eng. Sci.*, **37**, PP 803-830(1999).
13. Voyiadjis G.Z., Deliktas B., "A Coupled Anisotropic Damage Model for the Inelastic Response of Composite Materials", *Comput. Methods Appl. Mech. Eng.*, **183**, PP 159-199(2000).
14. Kattan P.I. and Voyiadjis G.Z., "Micromechanical Modeling of Damage in Uniaxially Loaded Unidirectional Fiber-Reinforced Composite Lamina", *Int. J. Solids Struct.*, **30**, PP 19-36(1993).
15. Barbero E., De Vivo L., "A Constitutive Model for Elastic Damage in Fiber-Reinforced PMC Lamina", *Int. J. Damage Mech.* , **10**, PP 73-93(2001).
16. Barbero E., Lonetti P., "An Inelastic Damage Model for Fiber Reinforced Laminates", *J. Composite Mater.*, **36**(8), PP 941-962(2002).
17. Lonetti P., Zinno R., Greco F., and Barbero E., "Interlaminar Damage Model for Polymer Matrix Composites", *J. Composite Mater.*, **37**(16), PP 1485-1504(2003).
18. Belytschko T., Liu W.K., Moran B., *Nonlinear Finite Elements for Continua and Structures*, John Wiley and Sons Ltd., New York, (2000).
19. Herakovich C.T., *Mechanics of Fibrous Composites*, John Wiley, New York, (1998).